

This is the accepted manuscript made available via CHORUS. The article has been published as:

Experimental Validation of the Two-Plasmon-Decay Common-Wave Process

D. T. Michel, A. V. Maximov, R. W. Short, S. X. Hu, J. F. Myatt, W. Seka, A. A. Solodov, B. Yaakobi, and D. H. Froula

Phys. Rev. Lett. **109**, 155007 — Published 12 October 2012

DOI: [10.1103/PhysRevLett.109.155007](https://doi.org/10.1103/PhysRevLett.109.155007)

Experimental validation of the two-plasmon-decay common-wave process

D. T. Michel,* A. V. Maximov, R. W. Short, S. X. Hu,
J. F. Myatt, W. Seka, A. A. Solodov, B. Yaakobi, and D. H. Froula
Laboratory for Laser Energetics, University of Rochester, Rochester, NY 14636

The energy in hot electrons produced by the two plasmon decay (TPD) instability, in planar targets, is measured to be the same when driven by one or two laser beams and significantly reduced with four for a constant overlapped intensity on the OMEGA EP. This is caused by multiple beams sharing the same common electron-plasma wave. A model, consistent with the experimental results, predicts that multiple laser beams can only drive a resonant common TPD electron-plasma wave in the region of wavenumbers bisecting the beams. In this region, the gain is proportional to the overlapped laser beam intensity.

PACS numbers: 52.38.Kd, 41.75.Jv, 52.35.Mw
Keywords:

Direct-drive inertial confinement fusion requires multiple overlapping laser beams that can then drive the two-plasmon-decay (TPD) instability. TPD creates large-amplitude electron plasma waves in the region near quarter-critical density [1]. These plasma waves can lead to anomalous absorption and hot-electron generation [2, 3] that can preheat the fusion fuel and reduce the compression efficiency. Understanding the behavior of TPD is critical to mitigating it in inertial confinement fusion experiments.

The TPD instability consists of the decay of an electromagnetic wave into two electron-plasma waves [4, 5]. Phase matching, energy conservation, and the dispersion relations of the waves limit the instability to a small region near the quarter-critical density. Stability calculations of a single-plane electromagnetic wave show that the spatial growth rate of instability is proportional to the quantity IL_n/T_e , where I is the laser beam intensity, L_n is the plasma density scale length, and T_e is the electron temperature of the plasma [6, 7]. When the instability is driven to nonlinear saturation, a broad spectrum of large-amplitude plasma waves is generated [8] and can accelerate electrons to high energies (~ 100 keV) [9].

When multiple overlapping laser beams with polarization smoothing are used [10], the total energy in hot electrons was shown to scale with the overlapped intensity (I_Σ), defined as the sum of the intensity of each beam [11]. This scaling would not be expected if the beams drive the TPD independently, according to the single plane wave growth rates. A model is proposed where different laser beams share a common-electron wave [12].

This Letter describes the first experimental validation of the common-wave process [Fig. 1(a)] where the total energy in hot electrons is measured to be similar when one or two polarized beams are used at the same overlapped intensity and significantly reduced when four beams with the same overlapped intensity are used. A theoretical description of the common-wave process shows that multiple laser beams can share an electron-

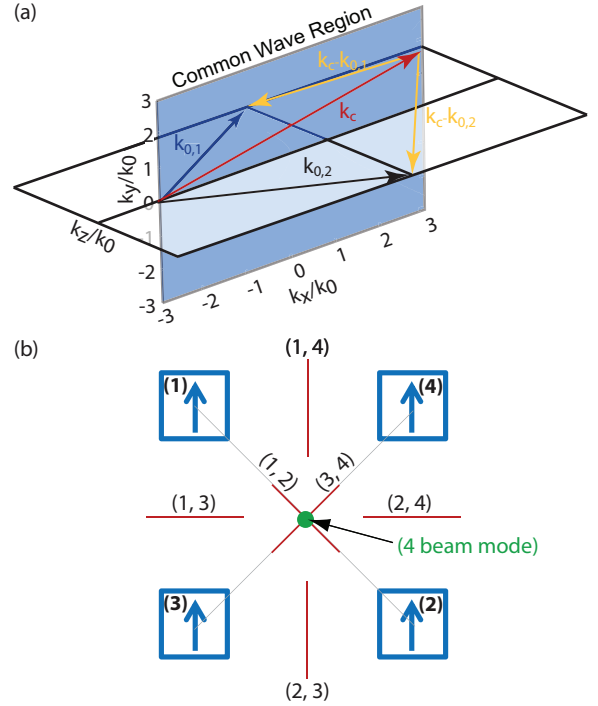


FIG. 1: (a) Schematic of the common-wave region for two beams: Two laser beam of wave vectors $k_{0,1}$ and $k_{0,2}$ share the common-plasma wave k_c located in the bisecting plane fulfilling the necessary condition $|k_c - k_{0,1}| = |k_c - k_{0,2}|$ independent of the polarizations of the laser beams; (b) Schematic of the seven common wave regions when four beams are used: six two beam common-wave planes (red lines) and one four beam common-wave line (green point).

plasma wave in the region bisecting the electromagnetic wave vectors. In this region, the temporal growth rate and convective gain of the dominant mode are proportional to the overlapped intensity, a factor that depends on the geometry, the polarization, and the relative intensity of the laser beams.

The experiments were conducted on OMEGA EP [13], where the four 351-nm beams are polarized vertically and

intersect the target at an angle of 23° with respect to the target normal [Fig. 1(b)]. The beams are spatially overlapped to within $20\text{ }\mu\text{m}$ and used 2-ns flat-top laser pulses that are co-timed to within 50 ps. Two sets of distributed phase plates [10] were used ($890\text{-}\mu\text{m}$ diameter for beams 1 and 2 and $840\text{-}\mu\text{m}$ diameter for beams 3 and 4) to produce an $\sim 1\text{-mm}$ -diam super-Gaussian intensity distribution profile. A maximum single-beam energy of 2 kJ (2.6 kJ) was used on beams 1 and 2 (3 and 4), which provided a single-beam $I_{Max} = 1.6 \times 10^{14}\text{ W/cm}^2$ ($I_{Max} = 2.4 \times 10^{14}\text{ W/cm}^2$). The relative error in intensities is dominated by the shot-to-shot power measurements on each beam of less than 5%. This results in a maximum error in overlapped intensity of 10%.

The laser beams illuminated a $30\text{-}\mu\text{m}$ -thick CH layer deposited on $30\text{ }\mu\text{m}$ of Mo and backed with an additional $30\text{ }\mu\text{m}$ of CH. Hydrodynamic simulations using the 2D code *DRACO* [14] indicate that the laser light interacts with the first layer, producing a CH plasma with density and temperature profiles that depends only on the overlapped laser intensity. For the experimental conditions presented here, the hydrodynamic profiles near quarter-critical density reach a steady state after about 1.5 ns. After this time, the calculated quantity $I_{\Sigma,q}L_n/T_e$ varies by less than 10% where $I_{\Sigma,q}$ is the overlapped intensity at the quarter-critical density. When the overlapped laser intensity is increased from $1.5 \times 10^{14}\text{ W/cm}^2$ to $7 \times 10^{14}\text{ W/cm}^2$, the density scale length (L_n) increases from $260\text{ }\mu\text{m}$ to $360\text{ }\mu\text{m}$, the electron temperature (T_e) increases from 1.5 keV to 2.5 keV, and, due to absorption, the laser intensity at quarter-critical density is about equal to half of the vacuum intensity; the ratio L_n/T_e is nearly constant ($\approx 160\text{ }\mu\text{m/keV}$).

The x-ray spectrometer [15–17] is used to measure the energy emitted into the Mo K_α emission line (E_{K_α}) using an absolutely calibrated planar LiF crystal spectrometer that views the target from the laser incident side at an angle of 63° from the target normal [17]. The hard x-ray detector [18] measures the x-ray radiation generated by the hot electrons in the Mo above $\sim 40\text{ keV}$, $\sim 60\text{ keV}$, and $\sim 80\text{ keV}$ [18]. It allows the hot-electron temperature to be estimated using the exponentially decreasing x-ray energy in each channel. The relative error in the measurement of the hot electron temperature is 20%. Monte Carlo simulations using the code EGSnrc [19] are used to determine the total hot-electron energy (E_e) given the measured hot-electron temperature (T_{hot}) and the total energy in the K_α emission [17]. The relative error of 25% is dominated by measurement errors. Figure 2(a) shows that the dependence of the hot-electron temperature with the total energy in K_α is comparable when using one beam, two beams or four beams.

Figure 2(b) shows that the total laser energy (E_l) converted into hot electrons ($f_{hot} = E_e/E_l$) as a function of the overlapped intensity is similar when using one or two beams in the horizontal, vertical, or diagonal con-

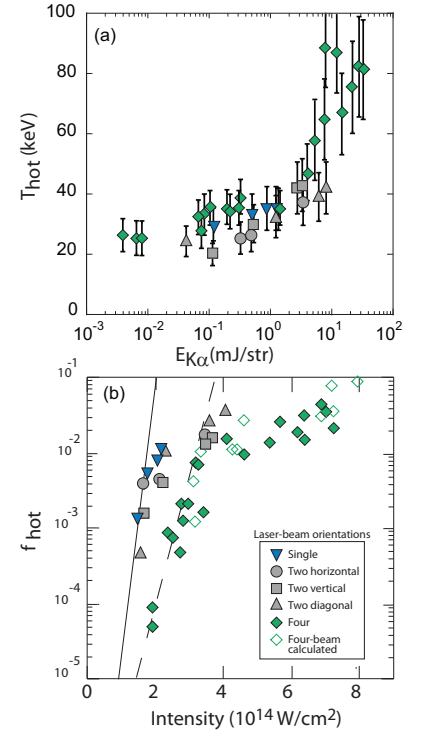


FIG. 2: (a) The measured hot-electron temperature is plotted as a function of the measured total energy in K_α for the five laser-beam orientations tested. (b) The fraction of laser energy converted to hot electrons (f_{hot}) is plotted as a function of the overlapped intensity. The four-beam hot electron generation is estimated (open diamonds) by multiplying the measured two-beam total hot-electron energy fraction by six and plotting the results at twice the two-beam intensity. The dashed line is a fit to the four beam data [$f_{hot} = 3 \times 10^{-8} e^{(8I_\Sigma/2)}$]. The solid line is scaled from the fit assuming the four beam results are dominated by the six two beam common wave modes driven at half of the intensity [$f_{hot} = 1 \times 10^{-8} e^{(8I_\Sigma)}$].

figuration and increases exponentially as a function of the overlapped intensity. These results show that the TPD growth is due to the interplay between the two beams through a common-wave process. If the hot electrons were generated by two independent single-beam processes, each with an intensity of $I_\Sigma/2$, the total hot-electron energy would be the sum of the hot-electron energy generated by each beam. This would be significantly smaller than the hot-electron energy generated by a single beam with $I = I_\Sigma$ (due to the measured exponential increase of the hot-electron energy with the laser intensity). The fact that the two beams produce similar total hot-electron fraction as a single beam shows that the common-wave process is very efficient.

When comparing the four-beam and single-beam results, Fig. 2(b) shows a significant decrease in the hot-electron energy for a given overlapped intensity (up to two orders of magnitude for $I_\Sigma \sim 2 \times 10^{14}\text{ W/cm}^2$). This reduction in the four beam experiments can be explained

heuristically on the basis of the two beam experimental results. The addition of the hot-electron fractions measured for six possible two beam configurations, plotted at twice the overlapped intensity, is consistent with the fraction of hot electrons measured when four beams are employed; see open symbols in Fig. 2(b). This suggests that the hot electrons generated by four beams are the result of the sum of the hot electrons generated by six independent two-beam interactions; i.e., the hot-electrons generated by the interaction between all four beams is not dominant.

The well-known theory of TPD [4, 5] is based on the dispersion relation for the two electron-plasma waves with frequency and wave vectors (ω, \mathbf{k}) and $(\omega - \omega_0, \mathbf{k} - \mathbf{k}_0)$, where ω_0 and \mathbf{k}_0 are the frequency and wave vector of the initial electromagnetic wave [4, 5]. In the case of multiple laser beams driving a common electron-plasma wave (ω_c, \mathbf{k}_c) , the dispersion relation is $\omega_c^2 = \omega_{pe}^2 + 3\mathbf{k}_c^2 v_{th,e}^2$ and for the corresponding daughter waves $(\omega_c - \omega_0)^2 = \omega_{pe}^2 + 3(\mathbf{k}_c - \mathbf{k}_{0,i})^2 v_{th,e}^2$, where $v_{th,e}$ is the electron thermal velocity, ω_{pe} is the plasma frequency, and $\mathbf{k}_{0,i}$ (with a norm k_0 independent of i) is the wave vector of beam i . A mathematical definition for the region where a resonant common-wave process exists is determined by satisfying the dispersion relations for all laser beams, $\cos(\mathbf{k}_c, \mathbf{k}_{0,i}) = \text{const}$, for $i = 1 \dots n$. For a two-beam configuration, this defines a plane in k -space bisecting the wave vectors of the two laser beams [Fig. 1(a)]. For more than two laser beams, this condition restricts the resonant common waves either to a line or eliminates them, depending on the laser beam symmetry. The four-beam growth rate in this experiment is restricted to a line [Fig. 1(b)].

The dispersion relation for the common-wave process is derived following the TPD linear theory [4, 5] for the conditions where the collision frequency is much smaller than the growth rate, satisfied for our experimental parameters: $D(\omega_c, \gamma, |\mathbf{k}_c|) = -\sum_i \frac{\gamma_{0,i}^2}{D(\omega_c - \omega_0, \gamma, |\mathbf{k}_c - \mathbf{k}_{0,i}|)}$, where γ is the temporal growth rate, $D(\omega, \gamma, |\mathbf{k}|) = \{[1 - \frac{\omega_{pe}^2}{\omega^2} (1 + 3k^2 \lambda_{De}^2)] \frac{\omega}{2} + i\gamma\}$ is the dispersion relation and $\lambda_{De} = \frac{v_{th,e}}{\omega_{pe}}$ is the Debye length. The single-beam homogeneous growth rate calculated in the common-wave region is $\gamma_{0,i}^2 = (\gamma_0^2)_{Max}^{SB} \cos^2(\alpha_i) f_c \beta_i$, where α_i is the angle between the polarization vector and the common-wave vector, $f_c = \left(\frac{k_c^2 - (\mathbf{k}_c - \mathbf{k}_{0,i})^2}{k_{0,i} |\mathbf{k}_c - \mathbf{k}_{0,i}|}\right)^2$, $\beta_i = \frac{I_i}{I_\Sigma}$, I_i is the intensity of the laser beam i , $(\gamma_0^2)_{Max}^{SB} = \frac{2}{c n_c m_e} \left(\frac{k_0}{2}\right)^2 I_\Sigma$ is the maximum single-beam homogeneous growth rate squared calculated for the overlapped intensity, c is the light velocity, m_e is the electron mass, $n_c = \frac{m_e \omega_0^2}{4\pi e^2}$ is the critical density, and e is the electron charge. To evaluate the maximum value of the growth rate, the minimum value of $D(\omega, \gamma, |\mathbf{k}_c - \mathbf{k}_{0,i}|)$ is determined by ensuring that the dispersion relations for all daughter waves are

satisfied. It follows that $D(\omega, \gamma, |\mathbf{k}_c - \mathbf{k}_{0,i}|) = i\gamma = \text{const}$ and the resonant common-wave growth rate is given by $(\gamma_0^2)^{MB} = \sum_i \gamma_{0,i}^2$. A geometric function is given by normalizing the multiple-beam growth rate squared to the maximum single-beam growth rate squared,

$$(\Gamma_0^2)^{MB} = \frac{(\gamma_0^2)^{MB}}{(\gamma_0^2)_{Max}^{SB}} = f_c \sum_i \cos^2(\alpha_i) \beta_i \quad (1)$$

The dominant mode is determined by the maximum of the geometric function which is a geometric factor $(f_g = (\Gamma_0^2)_{Max}^{MB})$ that depends only on the geometry of the laser beams, their polarizations, and their intensities relative to the overlapped intensity.

Figure 3(a)-(b) shows the calculated geometric functions for two beams $[(\Gamma_0^2)^{2B}]$ polarized perpendicular and parallel to the plane defined by the laser beams $(\mathbf{k}_{0,1}, \mathbf{k}_{0,2})$. The geometric functions calculated in k -space are significantly different as a result of the difference in the polarization vectors relative to the common-wave plane, although the geometric factor is similar for the two cases $[(\Gamma_0^2)_{Max}^{2B} \sim 1]$. The fact that the growth rates are the same explains why the total hot-electron energy is measured to be similar in the horizontal and vertical laser-beam configurations. For the configuration with two horizontal beams [Fig. 3(a)], the geometric function in the common-wave plane form two modified hyperbolas defined by $(k_y/k_0)^2 = (k_x/k_0) [(k_x/k_0) / \cos^2(\theta/2) - 1]$, where θ is the angle between the two laser beams. The geometric function decreases rapidly with k_y/k_0 , corresponding to the rapid decrease of the single-beam growth rates.

Figure 3(c) shows the four-beam geometric function $[(\Gamma_0^2)^{4B}]$ plotted along the four-beam common-wave region located along the line bisecting the laser beams [Fig. 1(b)]. The maximum value is reached for $k_x/k_0 \sim 1.3$ and $k_y/k_0 \sim 0.3$ where $(\Gamma_0^2)_{Max}^{4B} = 0.5$. For the same overlapped intensity, the single-beam and two-beam homogeneous growth rates for the dominant mode are similar $[(\Gamma_0^2)_{Max}^{2B} = 1]$, whereas the four-beam homogeneous growth rate for the dominant mode is decreased by a factor of 2 $[(\Gamma_0^2)_{Max}^{4B} = 0.5]$. These calculations support the experimental findings [Fig. 2(b)] where the single and two beam hot electron fractions are comparable, while the four-beam hot electron fraction is smaller.

To estimate the common-wave convective gain (in intensity), the maximum common-wave homogeneous growth rate is used in the formalism derived in Refs. [6, 20], $G = \frac{16\pi}{9} \left(\frac{v_{th,e}^2}{c^2}\right)^{-1} k_0 L \left[\frac{(\gamma_0^2)_{Max}^{MB}}{\omega_0}\right]^2$. The maximum common-wave gain for each configuration is,

$$G_c = 6 \times 10^{-2} \frac{I_{\Sigma,g} L_n \lambda_0}{T_e} f_g \quad (2)$$

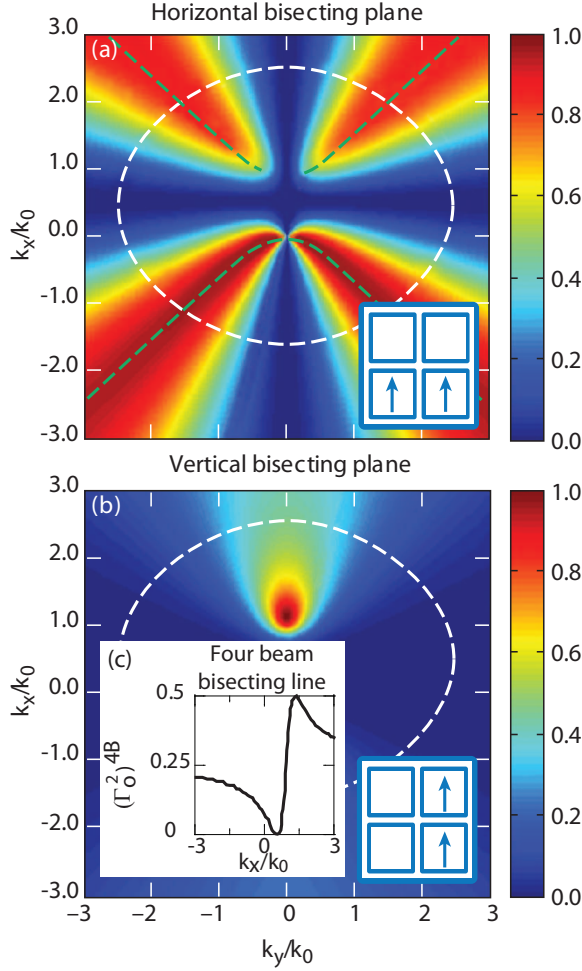


FIG. 3: Calculation of $(\Gamma_0^2)^{2B}$ in the common-wave plane for (a) two beams polarized perpendicular and (b) parallel to the plane $(\mathbf{k}_{0,1}, \mathbf{k}_{0,2})$. The dashed white lines correspond to the Landau cutoff ($k_{max}\lambda_{De} = 0.25$ where $k_{max} = \max[k_c, |\mathbf{k}_c - \mathbf{k}_{0,i}|]$) calculated for $T_e = 1.6$ keV, which defines the maximum wave vector for TPD [21]. The dashed green lines correspond to the two modified hyperbolas of maximum $(\Gamma_0^2)^{2B}$. (c) Calculation of $(\Gamma_0^2)^{4B}$ along the four-beam common-wave line. \mathbf{k}_x is along the projection of $\mathbf{k}_{0,i}$ in the common wave region, \mathbf{k}_y is perpendicular to \mathbf{k}_x , k_0 is calculated at quarter-critical density.

where T_e is in keV, $I_{\Sigma,q}$ is in 10^{14} W/cm², L_n is in μm , and λ_0 is in μm . For a given laser-beam configuration (relative beam angle and polarization), the common-wave gain is proportional to $I_{\Sigma,q}L_n/T_e$.

Figure 4 shows the hot electron fraction as a function of the calculated common-wave gain for the dominant mode [Eq. (2)]. When there are multiple common-wave regions, the dominant mode corresponds to the maximum common-wave gain. For all laser beam configurations, except for two diagonal beams, the hot electron fraction as a function of the gain is similar. For diagonal beams, the calculations underestimate the value of the gain.

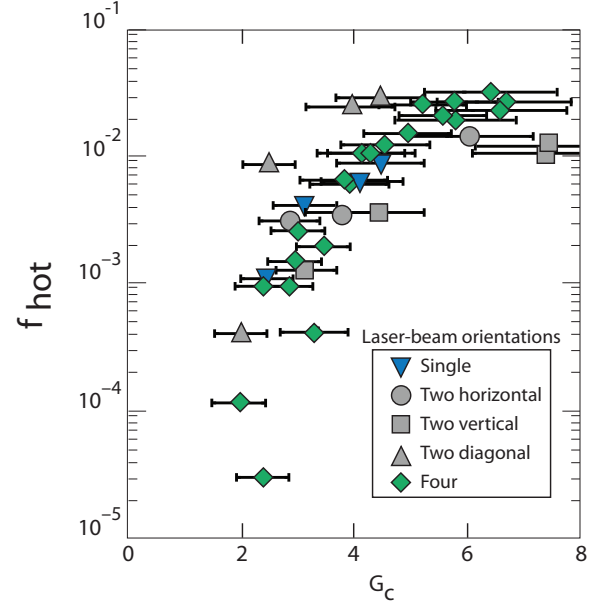


FIG. 4: The total hot electron energy divided by the laser energy is plotted as a function of the common-wave gain (G_c) for the dominant mode.

In summary, when maintaining the overlapped laser beam intensity, the total energy in hot electrons is measured to be similar when using one or two polarized beams and significantly reduced with four polarized beams. A linear common-wave model is consistent with these observations. For ignition designs, these results suggest that the common-wave process can be reduced by limiting the number of beams that are symmetric to one another or by reducing the geometric factor.

This work was supported by the U.S. Department of Energy Office of Inertial Confinement Fusion under Cooperative Agreement No. DE-FC52-08NA28302, the University of Rochester, and the New York State Energy Research and Development Authority. The support of DOE does not constitute an endorsement by DOE of the views expressed in this article.

* Electronic address: tmic@l1e.rochester.edu

- [1] H. A. Baldis *et al.*, Phys. Rev. Lett. **47**, 1658 (1981).
- [2] N. A. Ebrahim *et al.*, Phys. Rev. Lett. **27**, 1179 (1980).
- [3] R. L. Keck *et al.*, Phys. Fluids **27**, 2762 (1984).
- [4] M. V. Goldman *et al.*, Ann. Phys. (N.Y.) **38**, 117 (1966).
- [5] C. S. Liu *et al.*, Phys. Fluids **19**, 967 (1976).
- [6] M. N. Rosenbluth *et al.*, Phys. Rev. Lett. **29**, 565 (1972).
- [7] A. Simon *et al.*, Phys. Plasmas **26**, 3108 (1983).
- [8] J. Myatt *et al.*, Phys. Plasmas **19**, 022707 (2012).
- [9] D. H. Froula *et al.*, Phys. Rev. Lett. **108**, 165003 (2012).
- [10] T. J. Kessler *et al.*, in Laser Coherence Control: Technology and Applications, edited by H. T. Powell and T. J. Kessler (SPIE, Bellingham, WA, 1993) **1870**, 95104

- (1993).
- [11] C. Stoeckl *et al.*, Phys. Rev. Lett. **90**, 235002 (2003).
 - [12] R. W. Short and J. F. Myatt, *53rd Annual Meeting of the American Physical Society* UO6.00012, (2011).
 - [13] J. H. Kelly *et al.*, J. Phys. IV France **133**, 75-80 (2006).
 - [14] P. B. Radha *et al.*, Phys. Plasmas **12**, 056307 (2005).
 - [15] B. Yaakobi *et al.*, Phys. Plasmas **7** 3714 (2000).
 - [16] B. Yaakobi *et al.*, Phys. Plasmas **12**, 062703 (2005).
 - [17] B. Yaakobi *et al.*, Phys. Plasmas **19**, 012704 (2012).
 - [18] C. Stoeckl *et al.*, Rev. Sci. Instr. **72**, 1197 (2001).
 - [19] I. Kawrakow *et al.*, code EGSnrc [I. Kawrakow, D. W. O. Rogers, NRC Reports PIRS-701, (Ottawa:NRC) 2003).
 - [20] R. Yan *et al.*, Phys. Plasmas **17**, 052701 (2010).
 - [21] W. Seka *et al.*, Phys. Plasmas **16**, 052701 (2009).